Journal of Hydrology 592 (2021) 125748

Contents lists available at ScienceDirect

Journal of Hydrology

journal homepage: www.elsevier.com/locate/jhydrol

Research papers

Environmental isotopes ($\delta^{18}O$, $\delta^{2}H$, ^{222}Rn) and hydrochemical evidence for understanding rainfall-surface water-groundwater transformations in a polluted karst area

Wenjing Qin [a,c], Dongmei Han [a,b,c,*], Xianfang Song [a,b,c], Shaohua Liu [d,e,f]

[a] Key Laboratory of Water Cycle & Related Land Surface Processes, Institute of Geographic Sciences and Natural Resources Research, Chinese Academy of Sciences, Beijing 100101, China
[b] College of Resources and Environment, University of Chinese Academy of Sciences, Beijing 100049, China
[c] Sino-Danish College, University of Chinese Academy of Sciences, Beijing 100049, China
[d] Institute of Karst Geology, Chinese Academy of Geological Sciences, Guilin 541004, China
[e] Ecosystem and Rocky Desertification Treatment Key Laboratory, Ministry of Natural Resources, Guilin 541004, China
[f] Key Laboratory of Karst Dynamics, Ministry of Natural Resources & Guangxi, Guilin 541004, China

ARTICLE INFO

This manuscript was handled by Corrado Corradini, Editor-in-Chief

Keywords:
Surface water-groundwater interaction
^{222}Rn, $\delta^{2}H$ and $\delta^{18}O$ isotopes
Karst water

ABSTRACT

The vulnerable karst water systems and the serious pollution issues in Southwest China have been facing tremendous challenges, especially when controlling processes of transformation in rainfall, surface- and groundwater (SW and GW) are poorly understood in such areas. In this study, transformation processes have been identified based on physical–chemical indicators (T, DO, EC, HCO_3^{2-}, SO_4^{2-}, Ca^{2+}, and Mg^{2+}), $\delta^{2}H$ and $\delta^{18}O$ isotopes, and ^{222}Rn activities in different water forms. The $\delta^{2}H$ and $\delta^{18}O$ isotopic signals of the river are depleted in the upstream non-karst area due to the altitude effect. The karst aquifers are dominantly recharged by local rainfall in summer and by river water from the non-karst area in winter indicated by the seasonal variation of stable isotopic compositions. A ^{222}Rn mass-balance model was constructed to estimate GW-SW exchange during the autumn period. Net gaining and net losing sections (including a segment of conduit flow) were identified to be fluxes of 3.6×10^{-3} and -4.0×10^{-3} $m^3\ s^{-1}\ m^{-1}$ respectively. The bank storage water contributed critically in the net gaining section, deduced by the inconsistent responses of stable isotopic and chemical tracers to the GW influent, which resulted in a relative identical amount of influent and effluent water (5.0×10^{-3} and -1.4×10^{-3} $m^3\ s^{-1}\ m^{-1}$ respectively). In the net losing section (influent and effluent are 2.8×10^{-4} and -4.2×10^{-3} $m^3\ s^{-1}\ m^{-1}$ respectively), interactions through the segment of surface flow are sluggish, which is standing in stark contrast to the well-mixed flow in the conduit segment. The results reveal various signs of sulfides oxidation from the mine and tailings, along with liberated metals could be introduced and travelled across in the transformations of rainfall-SW-GW. It needs to put more efforts into the research of water quality and transport of metals hereafter.

1. Introduction

Karst aquifers supply drinking water to around a quarter of the global population (Ford and Williams, 2007). Southwest China is one of the world's most spectacular examples of humid tropical to subtropical karst landscapes (UNESCO World Heritage Centre, 2007). It is also regarded as one of the most prioritized regions to control the contamination of heavy metals attributed to historical mining (Li et al., 2014). Acid mine drainage caused by metal (s) ore exploration has become a long-standing problem that profoundly deteriorates the surface water (SW) and groundwater (GW) quality and aquatic biota (Sun et al., 2013). Besides, trace elements such as lead (Pb), zinc (Zn) and cadmium (Cd) liberated from historical mining, tailing deposits and then stored in soils and stream (or cave streams) sediments, have become the potential second contaminants sources to water systems (Gutiérrez et al., 2016). Enhanced transport of heavy metals driven by hydraulic forces such as

* Corresponding author at: Key Laboratory of Water Cycle & Related Land Surface Processes, Institute of Geographic Sciences and Natural Resources Research, Chinese Academy of Sciences, Beijing 100101, China. (D. Han).
E-mail address: handm@igsnrr.ac.cn (D. Han).

https://doi.org/10.1016/j.jhydrol.2020.125748
Received 9 October 2020; Received in revised form 4 November 2020; Accepted 5 November 2020
Available online 16 November 2020

leaching and storm flow has been observed widely (Mikkelsen et al., 1997; Wijngaard et al., 2017; Xiao et al., 2019; Aghili et al., 2018). The contaminated aquifers can be responsible for acting as long-term significant pollution sources to the surrounding environment (Wang et al., 2019).

The transformations from rainfall to surface- and ground-water, and the interactions between surface- and ground-water, are principally controlled by geomorphologic, hydrogeologic, and climatic conditions (Tóth, 1970; Sophocleous, 2002). Water in karst aquifers is fast diffusive and sometimes the infiltration is concentrated depends on the distribution of conduits, development of the heterogeneity and anisotropy (Parise et al., 2018). It is highly vulnerable to contamination and difficult to manage because of the unique hydrogeological characteristics. Contaminants such as metals move along and spread across water forms in karst areas, having chemical, physical and biological reactions with the surroundings under a highly dynamic and heterogeneous framework, which can affect the mobility, persistence, and potential exposure of humans and wildlife (Padilla and Vesper, 2018). The type of recharge also determines the fate of the metals, i.e. whether sedimented or transported in the conduits system (Vesper, 2019). Hydrologic connectivity in karst reservoirs has been poorly understood in contrast to other porous-medium aquifers (Bailly-Comte et al., 2009). It still has great challenges and uncertainty when trying to trace transportation, implement remedial actions, and manage contaminated systems (Padilla and Vesper, 2018). In order to develop protection strategies against water pollution, it is necessary to identify the different processes of transformation in rainfall-GW-SW.

Environmental tracers have become powerful and well-developed tools for investigating the governing processes of rainfall-SW-GW transformation in the karst water system. Thereinto, $\delta^{18}O$ and $\delta^{2}H$ stable isotopes and radioactive isotope ^{222}Rn are the most useful ones for tracing groundwater origin and the related pathways (Clark and Fritz, 1997; Cook, 2013; Rugel et al., 2016; Arnoux et al., 2017; Bhat and Jeelani, 2018), estimating groundwater input into streams and fluxes between the fast-circulated karst streams and aquifers (Cook et al., 2003; Atkinson et al., 2015; Ortega et al., 2015; Zhao et al., 2018),

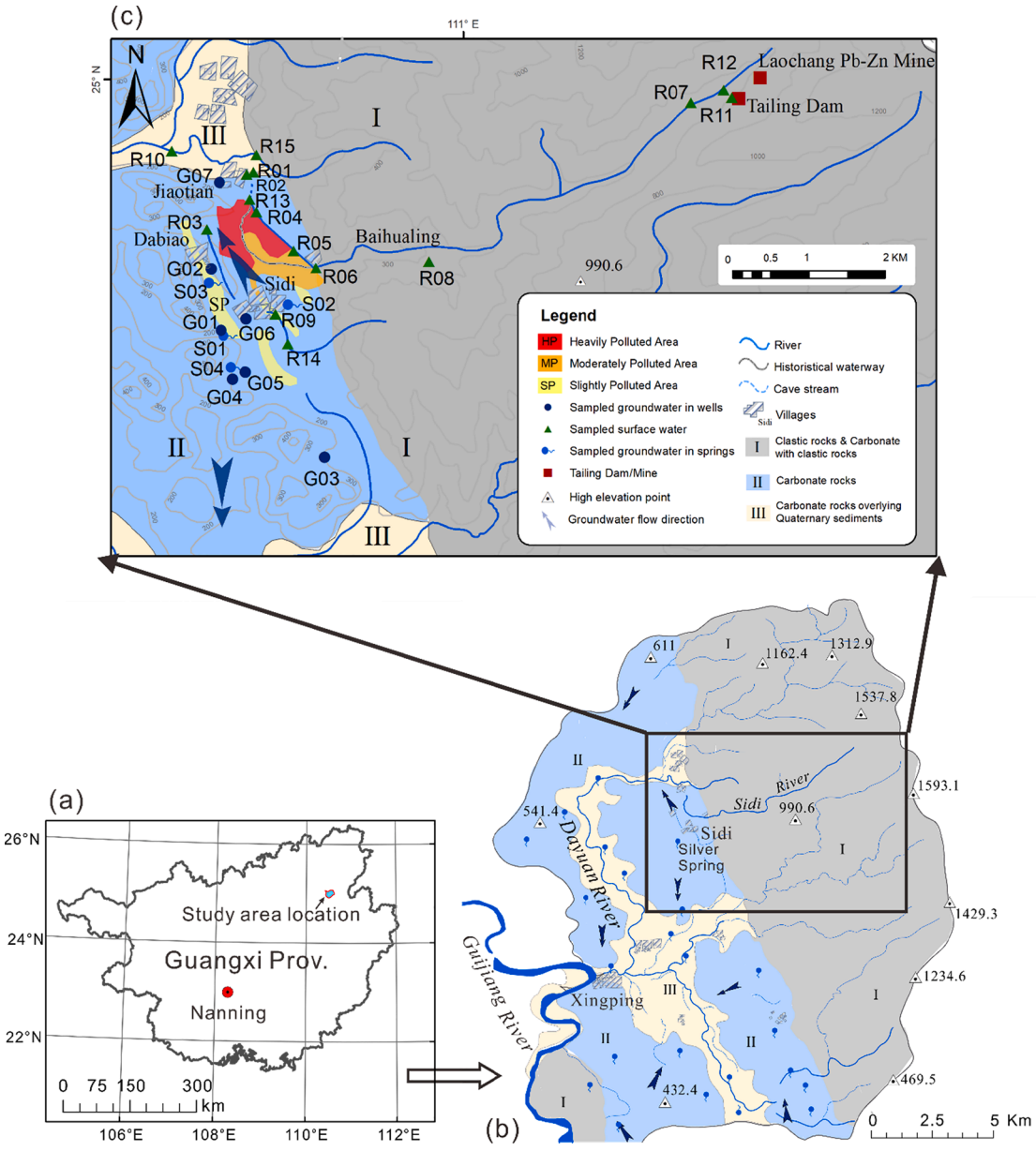

Fig. 1. Location map showing (a) The Guangxi Zhuang Autonomous Region, (b) the regional hydrological setting, and (c) sampling sites in the study area. The slightly, moderately and heavily polluted areas are obtained according to Kong et al., (2018).

investigating river infiltration into adjacent alluvial aquifers (Close et al., 2014), and ascertaining of the mixing processes from different aquifers (Folger et al., 1997; Ortega et al., 2017). By using multiple environmental isotopes such as ^{18}O, ^{2}H, ^{222}Rn and ^{3}H, rainfall-SW-GW transformation processes have been studied in karst areas all over the world (Jie, 2007; Rugel et al., 2016; Chu et al., 2017; Bhat and Jeelani, 2018; Charlier et al., 2019).

The study area includes a karst valley and the upstream non-karst mountainous area, located in the Southwest China (Fig. 1). The Laochang Pb-Zn mine and it's tailings pond at the upstream have been operated for decades, causing serious heavy metals pollution in the downstream soil (Kong et al., 2018). There are several studies have been carried out to evaluate the pollution level in the different land-use type of soil, the effect on the microbial enzymatic activity of soil microorganisms (Jin et al., 2015; Li et al., 2015; Kong et al., 2018). However, few studies has been carried out for evaluating the quality of surface- and ground-water, and migration of heavy metals in the hydraulic system, which has been threatened by the contaminated soil and the upstream mine and tailing pond (Qin et al., 2019). In order to further ascertain the migration of toxic metals in the water system, this study aims to trace the transformation processes of rainfall-surface water-groundwater by using of $\delta^{18}O$, $\delta^{2}H$, ^{222}Rn isotopes and other basic chemical-physical indicators.

The objectives of this study are (i) to decipher the controlling processes during rainfall to the surface and groundwater transformations both in the non-karst and karst area, (ii) to evaluate and quantify the exchange between river water and karst groundwater at different flow sections of the karst valley, and (iii) to propose a conceptual model of the rainfall-surface water-groundwater transformation processes for the study area and analyze the potential transport pathways of the pollutants. It can provide fundamental knowledge of the water cycle framework for further tracing toxic metals transportation, and support the water resources management for local authorities.

2. Study area

The study area is located in the southeastern of Guilin City, Guangxi Zhuang Autonomous Region, Southwest China. It is a karst valley surrounded by the range of Haiyang Mountains to the east (elevation varies from 900 to 1500 m) and karst hills (500–600 m height) to the west (Fig. 1). Sidi river originates from Haiyang Mountain, in which the Pb-Zn mine located, and flows westward down to the villages of Baihualing and Sidi, then turns to the southward to villages of Dabiao and Jiaotian (Fig. 1). The villages' s elevation varies in 100–200 m. The Sidi River flows into a karst conduit at Jiaotian Village, turns to an underground river with a runoff modulus around 6 L/s/km^2, and flows out at 1 km distance to the north (Fig. 1). The length of the upper reach (east to west reach) is around 7.3 km and area of the downstream valley (south to north reach) is around 5 km^2. The study area belongs to the Guilin-Yangshuo Basin, which is characterized by a subtropical monsoon climate with two distinct periods of a cold–dry season (from September to March) and a hot-rainy season (from April to August). The average annual temperature and rainfall are around 18.9 °C and 1886 mm/year. Almost 70% of the total precipitation occurs in the rainy season. The average monthly precipitation varies from 50 mm in December to 359 mm in June, while the average temperature per month ranges from 7.9 °C in January to 28.2 °C in July (Guo et al., 2015).

The lithology of the study area consists of Cambrian-Devonian (Є-D) sandstone and clastic rocks to the east Haiyang Mountain range (also simplified as "non-karst area" in this study), Devonian to Carboniferous (D-C) carbonate rocks, and Devonian (D) carbonates discontinuity covered by Quaternary (Q) clay and clay loam to the west (represented by "karst area", Fig. 1, Institute of Karst Geology, 2015). The relatively impervious formations of the non-karst area suggest that its recharge to the lowland karst area is mainly contributed by a focused surface water, i.e. the Sidi River (Fig. 1). Groundwater in the karst area generally flows from south to north and buried in depth within 10 m. Karst springs with discharges larger than 10 L/s during dry seasons are widely distributed. The overlying soil cover varies from 0 to 2 m in the valley area and mainly consists of calcareous clay and clay loam with limited permeability. Yaji experimental site in Guilin with the similar geology and lithology setting and close distance (about 38 km) to the study area, has been built to explore the karst hydrology processes since the 1990s (Yuan et al., 1990). Previous soil water movement experiments in around 45 cm depth (in 10 cm interval) on the Yaji experimental site showed the hydraulic conductivities of barren land vary in 0.0043–0.17 m/day with an average value of 0.06 m/day. In grasslands, the hydraulic conductivities are between 0.01 and 0.13 m/day with an average value of 0.05 m/day. While in shrublands the hydraulic conductivities range in 0.04–0.32 m/day with an average value of 0.07 m/day (Deng et al., 2017).

The study area has long suffered from heavy metals pollution (mainly Pb, Zn, Cd and Cu) in soils due to the exploration of the Pb-Zn mine since the 1950s (Fig. 1). The collapse of the tailings dam happened in the 1970s, which poured tailings sands and waste rocks directly down to the farmland of the Sidi village. Efforts including mining cessation, investigation and restoration of the soil pollution have been made and significantly decreases the concentration of metals in soil. However, the remains metals are still threatening the environment, e.g. the total Cd content of the soil is 40 mg/kg on average according to recent research (Li et al., 2015), which is still higher than 0.3 mg/kg, the Level II of soil environmental quality standard of China (GB15618—1995) (National Standard of the People's Republic of China, 2015; Lin, 1997, 1995). Moreover, the Sidi River continuously transports heavy metals to the downstream karst area presented by the previous study (Qin et al., 2019).

3. Material and methods

3.1. Water sampling and analysis

Previous investigations have been carried out in winter (December. 2015) and summer (June. 2016), in order to understand the general hydraulic and hydrogeology regime, and effects of the abandoned Pb-Zn mine on water quality of the study area (Qin et al., 2019). It is better to conduct the field investigation between previous seasons as a complementary under limit research conditions. Moreover, it is important to implement the SW-GW interaction survey during (also before and after) period without heavy precipitation to simplify the process of data collection and computation. As a result of above considerations, field measurement and sampling campaigns were conducted in the study area during the period of 23rd to 30th September. 2018. Besides, hydrochemical and $\delta^{2}H$ and $\delta^{18}O$ data for surface and groundwater collected from the previous research by Qin et al. (2019) on the study area in December. 2015 and June. 2016 have been compiled and compared with the data collected during September. 2018 in this study, through exactly the same analysis methods and data processing at the same lab.

Twenty-six water samples were collected, including 11 groundwater samples and 15 river water samples. Seven GW samples were taken from shallow domestic wells drilled in the karst aquifer with well depths ranging from 2 to 10 m. Groundwater sampling was performed using either a submersible pump or a hand pump that was pumping water at least 10 and 20 min respectively, before sampling to obtain fresh groundwater. The rest 4 GW samples were collected from karst springs. There are 11 SW samples were taken from the Sidi River and one of them (R08) were sampled from a tributary of the Sidi River on the non-karst area (Fig. 1). The remaining 4 were sampled from the karst spring or GW -fed streams. Spring and other surface water were sampled about 30 cm below the water surface, or in the middle of depth if the total depth is lower than 60 cm. The principle of surface- and groundwater sampling campaigns is following the flow direction of karst GW and the Sidi River. Samples for water chemistry analysis were infiltrated through 0.45 μm

filter immediately in situ, collected in three 100 ml HDPE bottles, which were overflowed and tightly capped protect from air contact, and stored at 4 °C fridge after sealed with parafilm. All samples were immediately transported to the laboratory for further analysis.

With the restriction of accessibility, R05, R04 and R01 sampling points are set as cross-sections in the exploration of SW-GW interaction as their well representativity. Velocity-area method was applied in determining the discharge of each cross-section (Herschy, 1998). A portable propeller current meter (LS10, China) with a detection range between 0.10 and 4.0 m/s with a precision of ≤1.5% was used in river flow velocity measurement at sampling points R05, R04 and R01. The oxidation–reduction potential (ORP, mV), electrical conductivity (EC, μS/cm), dissolved oxygen (DO, mg/L), pH, and water temperature (T, °C) were recorded in situ after stable values reached by a portable Multi-parameter water quality meter (WTW Multi 3420, Germany). The HCO_3^- and Ca^{2+} concentrations were titrated in situ using the Merck titration box (Germany). Radon measurements were conducted by slowly extracting 100 ml samples from sampling depth directly into air-tight glass bottles and then purging with air by a separate Alpha PUMP in a closed loop with a portable ^{222}Rn detector system Aqua KIT-Alpha PUMP-Alpha GUARD PQ2000PRO (Germany), via α-decay accounts. ^{222}Rn activities were measured over four 10-minute intervals with a detection range of 2–2,000,000 Bq/m^3 and the accuracy of 3%. More than three 10-minute intervals of air ^{222}Rn activities were measured between two water samples measurement to ensure the equipment reached the background value. Taking the average value of readouts for each sample and converted to ^{222}Rn activities in water according to (Rößler and Villert, 2017):

$$c_{water} = c_{readout} \times \left(\frac{V_{system} - V_{sample}}{V_{sample}} + k\right) - c_0 \times \left(\frac{V_{system} - V_{sample}}{V_{sample}}\right) \quad (1)$$

where c_{water} represents ^{222}Rn activities in water samples, $c_{readout}$ represents ^{222}Rn activities read out from the detector. V_{system} is the total volume of air in the system, which is 1122 ml in this case. V_{sample} is the volume of water sample, which is 100 ml in this case. While k is the diffusion coefficient of ^{222}Rn in the system, when the temperature is between 10 and 30 °C, k is set as 0.26 with an error of ±2%.

Anions Cl^- and SO_4^{2-} were analyzed by ion chromatography (IC, ICS-2100, Dionex). Major cations Ca^{2+}, Na^{2+}, K^+, and Mg^{2+} were measured using a inductively coupled plasma optical emission spectrometer (ICP-OES, Optima 5300DV, Perkin-Elmer, USA) at the Institute of Geographic Sciences and Natural Resources Research (IGSNRR), China Academy of Sciences (CAS). Charge balance errors in all analyses were <8%. The detection limits for ICP-OES and IC were both 1 mg/L. Analytical precision for major ions was within 1%. δ^2H and δ^{18}O of the water samples were measured using an isotopic water analyzer (LGR, USA) at the Key Laboratory of Water Cycle and Related Land Surface Process of IGSNRR, CAS. The δ^2H and δ^{18}O data are expressed as the parts per thousand deviations (‰) relative to Vienna Standard Mean Ocean Water (V-SMOW) with precisions of ±1‰ and ±0.1‰, respectively.

3.2. Mass balance of water flow and ^{222}Rn

3.2.1. Flow mass balance

Rainfall and evaporation need to be considered in the balance of flow mass. The average annual evaporation rate in the Guilin area is 1378.3 mm (Deng et al., 2017), i.e. 3.78 mm/d. With a 5-day mean life of ^{222}Rn, the evaporation loss could be 18.8 mm, which is around 2.5%-2.7% of the river depth about 0.76–0.7 m along the calculated sections of the Sidi river (Table 3). Therefore, considering that the runoff times within the river sections are both less than one day, evaporation loss can be neglected in the mass balance equation. There was rarely precipitation in the study area before and after the sampling campaign. Hence, precipitation and evaporation can be neglected in the mass balance. Basic mass balance equations between the upstream and downstream reaches can be expressed by Equations (2) and (3) for river water flow:

$$Q_d = Q_u + q_n L \quad (2)$$

$$q_n = q_g - q_r \quad (3)$$

Q_u (m^3/s) and Q_d (m^3/s) are the discharge of the upstream, downstream respectively. While q_g and q_r theoretically represent the rate of groundwater inflow to the river and river water outflow to aquifer per unit length of river reach [m^3/(s·m)]. And q_n is the net value of q_g and q_r. A positive q_n means more groundwater recharge to the river compare with river water outflow, and *vice versa*. Only q_n can be calculated according to this river flow mass balance, instead of the specific q_g and q_r..

3.2.2. ^{222}Rn isotope mass balance

As an inert, naturally occurring, radioactive gas (3.8 days of half-life) produced by the radioactive decay of ^{226}Ra, ^{222}Rn diffuses into pore water and becomes concentrated in the aqueous phase (Ellins et al., 1990). ^{222}Rn in surface water derives from upstream flow, groundwater recharge, radioactive decay of ^{226}Ra, and hyporheic exchange of riverbed sediments. Once the sources and sinks of radon reach equilibrium in a unit water body, i.e. a steady state of environmental condition been reached, the radon activity does not change with time. The immediately increased ^{222}Rn activity in surface water can be considered as a signal of groundwater recharge. Subsequently, due to degas and radioactive decay, the elevated ^{222}Rn activity will gradually decrease to the equilibrium value (Yang et al., 2020). It is also assumed that both in longitudinal and vertical, radon in the water is instantaneously mixed and reach a stable state, water collected in the downstream is the same part that collected in the upstream and can represent the average value of the section (Cook, 2013).

Hyporheic exchange can increase the ^{222}Rn activity in the flow of the river without adding discharge, which could lead to the overestimation of the groundwater inflow (Cook et al., 2006; Cook, 2013). An elaborate investigation of hyporheic exchange requires meticulous research of the riverbed including a series of complex experiments (Cook, 2013). However, access to collect enough river sediments for the estimation of radon production, also for accurately measuring the porosity of the river sediments is limited due to the steep topography. Following the previous studies (Su et al., 2015; Zhao et al., 2018; Yang et al., 2020), for an area with sparse hydraulic data tests, the hyporheic exchange is not considered in this study.

According to the mass conservation theory that take both gas exchange and radioactive decay processes into account (Danckwerts, 1951; O'Connor and Dobbins, 1958), Su et al. (2015) developed a method to calculate the GW-SW exchange in three different exchange processes:

case A, only GW recharge to SW:

$$C_d > C_u \;\&\; Q_d > Q_u \quad (4)$$

case B, only SW losing to GW:

$$C_d < C_u \;\&\; Q_d < Q_u \quad (5)$$

and case C both processes occurred:

$$C_d > C_u \;\&\; Q_d < Q_u, \; or \; C_d < C_u \;\&\; Q_d > Q_u \quad (6)$$

This method can be applied in the presented study as it is able to give more specificity of the interaction processes:

$$C_d Q_d = \int_0^L q_g C_g e^{(-\alpha x)} d_x + C_u e^{(-\alpha L)} Q_u \quad (7)$$

$$C_d Q_d = C_u e^{(-\alpha L)} Q_u - \int_0^L q_r C_u e^{-\alpha(L-x)} d_x \quad (8)$$

$$\begin{cases} C_d Q_d = \int_0^L q_g C_g e^{(-\alpha L)} d_x + C_u\, e^{(-\alpha L)}\, Q_u - \int_0^L q_r \frac{(Cu + Cd)}{2} e^{-\alpha(L-x)} d_x \\ Q_d = Q_u + q_g L - q_r L \end{cases} \quad (9)$$

where:

C_u: ^{222}Rn concentrations of river water at the upstream sampling location (Bq/m^3)
C_d: ^{222}Rn concentrations of river water at the downstream sampling location (Bq/m^3)
C_g: ^{222}Rn concentration of the discharged groundwater (Bq/m^3)
q_g: the average groundwater discharge for the entire width and per length (m^3/m/s)
q_r: the average river discharge (m^3/m/s) for the entire width and per length (m^3/m/s)
α: total loss coefficient for ^{222}Rn (m^{-1})
L: distance between the two sampling locations along the river reach (m)
x: distance between the points at which the interaction process occurs and the downstream location (m)

The average water level and velocity are the arithmetic average of the upstream and downstream. Groundwater endmember is the arithmetic average of the samples most close to the two river sections (Fig. 1). Sample S03 and G02 for section R05-R04 and S03, G02 and G07 for the section R04-R01.

The total loss coefficient α refers to the arithmetic sum of decay constant corrected for the average river velocity β and the loss coefficient γ caused by gas exchange (Ellins et al., 1990):

$$\alpha = \beta + \gamma \quad (10)$$

The decay constant corrected for the average river velocity β can be expressed as (Ellins et al., 1990):

$$\beta = \lambda / v \quad (11)$$

where:

v: average velocity of river water (m/s)
λ: coefficient of ^{222}Rn radioactive decay, $\lambda = 2.08 \times 10^{-6}$ s^{-1}

There are two models for estimating ^{222}Rn gas exchange, the surface renewal theory (Danckwerts, 1951; O'Connor and Dobbins, 1958) and the stagnant film model (Broecker, 1982; Lewis and Whitman, 1924). The latter model assumes that a stagnant film of water separates the stream and the air above it, which is inapplicable in the study area as the Sidi River is mainly turbulent. When the gas exchange in a stream is mostly determined by turbulence, the renewal theory can be applied to estimate ^{222}Rn concentration loss (Stellato et al., 2008). Therefore, loss coefficient γ caused by gas exchange is (Danckwerts, 1951; O'Connor and Dobbins, 1958; Stellato et al., 2008):

$$\gamma = D^{\frac{1}{2}} / \left(h^{\frac{1}{2}} v^{\frac{3}{2}} \right) \quad (12)$$

where:

D: molecular diffusion coefficient for ^{222}Rn gas (m^2/s), -log$D$ = 980/T + 1.59, T is the absolute temperature with unit of K
h: average depth of river water (m)

In total, α can be expressed as:

$$\alpha = \lambda / v + D^{\frac{1}{2}} / \left(h^{\frac{1}{2}} v^{\frac{3}{2}} \right) \quad (13)$$

The ^{222}Rn model is based on constant-value parameters, which fluctuates along the river. Therefore, it is necessary to examine the errors caused by variation of parameters (Lenhart et al., 2002). Sensitivity analysis of parameters was applied to obtain the level of accuracy if various parameters used in the calculation, and to reduce the uncertainty based on a better consideration of the ^{222}Rn mass balance equations (Su et al., 2015). Eq. (14) can be used to evaluate the relative error (δ) of calculation results due to different levels ($\Delta x = \pm 1\%, \pm 1\%, \pm 5\%, \pm 10\%, \pm 20\%, \pm 35\%, \pm 50\%$) of uncertainties of each parameter:

$$\delta = |y(x_0 + \Delta x) - y(x_0)| / y(x_0) \times 100 \quad (14)$$

where x is the sensitive parameter, y is the calculated result.

4. Results

4.1. Physical and hydrochemical characteristics of water samples

Physical and hydrochemical parameters of water samples, including water temperature, pH, DO, EC, and ORP, are presented in Table 1. Water temperature measured for surface and groundwater samples ranged between 19.9 and 26.4 °C and 20.7–25.1 °C with average values of 22.4 and 22.3 °C, respectively. Values of pH have a range of 7.6–8.5 with an average value of 8.0 for surface water and slightly acid (6.7–7.9 with an average value of 7.3) for groundwater. Apparently, DO in the Sidi River (varied between 4.5 and 8 mg/L with an average value of 6.9 mg/L) is larger than that in groundwater (varied in 1.2–6.2 mg/L with an average value of 4 mg/L). EC values ranged from 82.9 to 467.2 μS/cm in the surface water with an average value of 244.1 μS/cm. Karst groundwater samples have relatively higher EC with a range of 213–631.6 μS/cm and an average value of 457.9 μS/cm.

Major chemical components of surface- and ground-water samples and the water types can be seen from Table 2 and 5, and Piper plot (Fig. 2). The data collected from the previous research (December. 2015 and June. 2016) are also compiled in Fig. 2. Most of surface and groundwater were dominated by Ca-HCO_3 type, except for those taken from the Sidi River with a higher percentage of sulfate and dominated by Ca-SO_4 or Ca-HCO_3·SO_4 type. The discharge of the Sidi River significantly increased from 0.34 m^3/s at R07 to 3.77 m^3/s at R04, then decreased to 0.02 m^3/s at R01, the outlet of the conduit (Fig. 5). Variations of EC, HCO_3^{2-}, SO_4^{2-}, Ca^{2+}, Mg^{2+}, DO, and temperature along the SW and GW flow are shown in Figs. 4 and 7,. Water from the upstream of the Sidi River is characterized by relative lower chemical constituents except for SO_4^{2-}.

4.2. Isotopes (δ^2H, δ^{18}O and ^{222}Rn) in surface water and groundwater

The statistical results of δ^{18}O and δ^2H and the plot of δ^{18}O versus δ^2H for surface water and karst groundwater are shown in Table 2 and Fig. 3, respectively. The δ^{18}O values in surface water samples ranges from −7.4‰ to −5.8‰ (average value of −6.6‰) and δ^2H values from −43‰ to −33‰ (average value of −38‰). δ^{18}O values in groundwater ranged from −6.1‰ to −5.2‰ with an average of −5.8‰ and δ^2H values from −38‰ to −30‰ with an average of −34‰, respectively (Table 2). Most of the samples taken from the upstream of the Sidi River are characterized by lighter δ^{18}O and δ^2H isotopic signals thus located in the bottom-left corner of the blue area in Fig. 3. While δ^{18}O and δ^2H are heavier in karst groundwater in the downstream area (including karst spring water, karst spring-fed streams and well water from karst aquifer) thus located in the red circle of the relative upper-right corner.

The variations of δ^{18}O, δ^2H and EC along the SW and GW flow are shown in Fig. 4. Water from the upstream of the Sidi River characterized with a relative depleted isotopic signal (δ^2H is around −40‰ and δ^{18}O is around −7.0‰) until it flew into the conduit at sampling point R13 (δ^2H is −34‰ and δ^{18}O is −5.9‰). Tributary of the Sidi River like R08 (δ^2H is −34‰ and δ^{18}O is −6.0‰) are at relatively lower elevation thus carried

Table 1
Physical and chemical indicators of surface water and groundwater.

	Units	N total	Mean	Standard Deviation	Minimum	Median	Maximum	N total	Mean	Standard Deviation	Minimum	Median	Maximum
		Surface water						Groundwater					
T	°C	15	22.37	1.89	19.87	21.63	26.40	11	22.33	1.18	20.71	22.08	25.10
EC	μs/cm	15	244.06	125.72	82.89	195.10	467.20	11	457.88	112.34	213.00	485.80	631.60
ORP	mv	15	187.51	27.36	131.10	188.90	227.10	11	201.13	15.22	179.10	201.00	229.70
pH	–	15	8.01	0.23	7.64	7.95	8.46	11	7.27	0.30	6.73	7.20	7.91
DO	mg/L	15	6.91	0.93	4.50	7.15	7.99	11	3.97	1.64	1.24	4.05	6.19
TDS	mg/L	15	85.54	31.18	35.65	75.27	135.18	11	148.18	39.22	61.74	149.74	226.06

Table 2
Major chemical ions, alkalinity and stable isotopic values of surface water and groundwater.

	Units	N total	Mean	Minimum	Median	Maximum	N total	Mean	Minimum	Median	Maximum
		Surface water					Groundwater				
Ca^{2+}	mg/L	15	32.7	14	18	80	11	79.64	20	88	116
Mg^{2+}	mg/L	15	18.26	9.97	18.56	24.08	11	15.33	7.21	12.02	26.72
$Na^{+}+K^{+}$	mg/L	15	6.25	3.00	5.78	11.31	11	5.68	0.57	3.75	21.61
Cl^{-}	mg/L	15	1.84	1.01	1.41	4.36	11	1.89	0.57	1.34	5.76
SO_4^{2-}	mg/L	15	16.27	2.88	17.83	38.40	11	5.31	1.98	5.10	12.29
Alkalinity	mg/L	15	153.26	91.5	115.9	298.9	11	281.7	158.6	298.9	353.8
$\delta^{18}O$	‰	15	−6.6	−7.4	−6.8	−5.8	11	−5.8	−6.1	−5.8	−5.2
$\delta^{2}H$	‰	15	−38	−43	−40	−33	11	−34	−35	−34	−30

Table 3
Exchange fluxes of surface water and groundwater according to ^{222}Rn mass balance.

Samples/Sections	Q	T	$\bar{h}$	$\bar{v}$	L	Rn^{222}	Rn^{222} gw endmember	$q\_^{222}Rn$		q_n
Units	m^3/s	K	m	m/s	m	Bq/m^3	Bq/m^3	$m^3\ s^{-1}\ m^{-1}$		$m^3\ s^{-1}\ m^{-1}$
								q_g	q_r	
R05	0.3429	296.73				12,150				
R05-R04			0.76	1.27	958		2303.4	5.01×10^{-3}	-1.43×10^{-3}	3.58×10^{-3}
R04	3.7725	296.93				159.5				
R04-R01			0.70	0.72	950		4785.6	2.80×10^{-4}	-4.23×10^{-3}	-3.95×10^{-3}
R01	0.0157	299.56				453				

NOTE: q_n is the net exchange calculated by q_g minus q_r, a positive value of q_n represents the average groundwater discharge for the entire width and per length of the river, $m^3/(s{\cdot}m)$; a negative q_n value means average river leakage for the entire width and per length of the river, $m^3\ s^{-1}\ m^{-1}$.

Table 4
Relative error of calculated results for ^{222}Rn mass balance.

Measurement error		C_u	C_d	C_g	Q_u	Q_d	L	T	v	h
Relative error	−50%	120.7%	19.4%	56.5%	16.7%	40.7%	97.2%	73.3%	9.1%	33.9%
	−35%	49.6%	13.5%	35.4%	11.3%	28.5%	51.7%	51.6%	5.6%	17.4%
	−20%	18.9%	7.7%	19.3%	6.4%	16.3%	23.8%	26.5%	2.7%	8.0%
	−10%	7.5%	3.9%	9.6%	3.1%	8.1%	10.5%	11.9%	1.2%	3.6%
	−5%	3.4%	1.9%	4.8%	1.6%	4.1%	5.0%	5.7%	0.6%	1.7%
	−1%	0.6%	0.4%	1.0%	0.3%	0.8%	1.0%	1.1%	0.8%	0.3%
	1%	0.6%	0.4%	1.0%	0.3%	0.6%	1.0%	0.9%	0.8%	0.1%
	5%	2.6%	1.7%	4.5%	1.3%	2.5%	4.7%	4.3%	4.1%	0.5%
	10%	5.0%	2.8%	8.4%	1.8%	4.2%	7.8%	4.5%	8.0%	1.0%
	20%	8.9%	5.6%	17.6%	3.5%	8.4%	15.4%	8.2%	16.4%	1.9%
	35%	13.7%	9.0%	32.9%	5.2%	13.8%	25.2%	12.1%	30.2%	3.2%
	50%	17.4%	11.4%	50.7%	5.6%	18.0%	32.9%	14.3%	44.9%	4.2%

with $\delta^{18}O$ and $\delta^{2}H$ composition, which is close to the enriched karst groundwater. While $\delta^{18}O$ and $\delta^{2}H$ composition in karst streams like R09 and R14 are relatively depleted similar to that in the Sidi River (Fig. 4). Similar to $\delta^{18}O$ and $\delta^{2}H$, EC varied around 150 μS/cm in the Sidi River, which is significantly lower than that in the karst groundwater and increased at the outlet of the conduit.

A relatively distinct difference between SW and GW can be identified by the measured ^{222}Rn activities except for the peak value at R05 in the Sidi River. ^{222}Rn activities in GW ranged from 2216.7 to 21,000 Bq/m^3 with an average value of 8190.2 Bq/m^3, while for surface water, it varied from 159.5 to 12,150 Bq/m^3 with an average value of 3232.8 Bq/m^3. The variations of the ^{222}Rn activities along the Sidi River and the karst groundwater flow direction can be seen from Fig. 5. ^{222}Rn activities in groundwater are relatively low (e.g. sample G03 is 3770 Bq/m^3) at the south part of the study area, increased to the peak value of 21,000 Bq/m^3 at the sample point S02 and dropped to 2390 at G02 (GW flows from the south to north). Compared with karst groundwater, there are less ^{222}Rn activities in the tailings pond (1565 Bq/m^3, sample R11) as

Table 5
Concentrations of major ions and isotopic compositions for surface water and groundwater samples.

sampleID	^{222}Rn	δ^2H	δ^{18}O	Ca^{2+}	Mg^{2+}	Na^++K^+	Cl^-	SO_4^{2-}	HCO_3^-*
Units	Bq/m3	‰	‰	mg/L	mg/L	mg/L	mg/L	mg/L	mg/L
G01	4625	−35	−5.9	92	14.40	5.60	2.06	3.65	311.1
G02	2390	−30	−5.7	42	12.02	21.61	5.76	12.29	189.1
G03	3770	−30	−5.4	82	26.21	0.57	0.57	2.26	335.5
G04	9120	−30	−5.2	96	9.64	2.66	1.09	4.59	292.8
G05	13,350	−36	−6.0	102	7.21	3.39	1.46	5.30	298.9
G06	7615	−38	−6.1	116	8.88	11.00	3.53	5.10	353.8
G07	9750	−33	−5.3	58	11.12	5.32	1.31	9.71	176.9
S01	9075	−37	−6.0	88	17.25	3.75	1.28	2.98	341.6
S02	21,000	−34	−5.9	20	26.72	4.41	1.56	5.34	158.6
S03	2217	−34	−5.9	86	26.62	0.93	0.85	1.98	353.8
S04	7180	−33	−5.8	94	8.56	3.23	1.34	5.17	286.7
R01	453	−33	−5.8	80	20.12	3.00	1.14	2.96	298.9
R02	453.3	−34	−6.1	74	15.31	7.96	2.06	2.98	280.3
R03	311.5	−42	−6.9	76	15.02	6.78	2.02	2.93	280.3
R04	159.5	−41	−6.9	16	20.50	5.42	1.32	32.06	97.5
R05	12,150	−40	−6.9	14	21.83	6.81	1.41	30.34	103.7
R06	7385	−43	−7.4	18	18.56	6.10	1.49	27.84	97.6
R07	4555	−40	−6.6	24	20.27	4.19	1.02	38.40	103.7
R08	2480	−34	−6.0	14	24.08	10.04	4.36	7.14	140.3
R09	9270	−39	−7.0	66	9.97	8.76	1.91	2.88	225.7
R10	6510	−43	−7.4	15	16.13	4.01	1.39	20.91	91.5
R11	1565	−42	−6.7	19	18.03	5.50	1.14	18.90	115.9
R12	1600	−41	−6.8	24	16.59	4.40	1.01	17.83	115.9
R13	943	−34	−5.9	18	19.54	5.78	1.32	30.86	97.5
R14	458.8	−35	−6.0	14	16.52	11.31	3.94	3.69	115.9
R15	197.7	−34	−5.9	18	21.48	3.67	2.05	4.31	134.2

* Alkalinity expressed as HCO_3^-.

well as in the upstream of the Sidi River. ^{222}Rn activities in the Sidi River reached the peak value of 12,150 Bq/m^3 at the sampling site R05 and decreased to lower than 1000 Bq/m^3 in the conduit flow (Fig. 5).

4.3. Estimation of SW-GW exchange

^{222}Rn activities and flow discharge were applied to determine the relationship of SW-GW interaction and quantify the net exchange and gross exchange in specific directions in sections R05-R04 and R04-R01. The net exchange of SW and GW was obtained according to the flow mass balance (Equation (2)). The endmember of GW for the section R05-R04 was the average value of ^{222}Rn activities in the karst groundwater along the river flow (S03 and G02), the same as the calculation of section R04-R01 (S03, G02 and G07). In the section R05-R04, the ^{222}Rn concentration of the downstream sampling site R04 is lower than at the upstream sampling site R05, and the river discharge of the downstream sampling site is higher than that of the upstream sampling site. Therefore, it was assumed that inflow from GW to river occurs in conjunction with river water outflow, i.e. case C, the same as the calculation of section R04-R01. The gross influent from groundwater q_g and gross effluent from the river q_r were estimated based on Eq. (9). Parameters and results for river sections are shown on Table 3. The net exchange q_n in section R05-R04 is 3.58 × 10^{-3} m^3 s^{-1} m^{-1}. The gross flux of inflow from groundwater q_g is 5.05 × 10^{-3} m^3 s^{-1} m^{-1}, and the outflow from river q_r is 1.43 × 10^{-3} m^3 s^{-1} m^{-1}. While the net exchange q_n in section R04-R01 is 3.95 × m^3 s^{-1} m^{-1} with the q_g of 2.80 × 10^{-4} m^3 s^{-1} m^{-1} and q_r of 4.23 × 10^{-3} of m^3 s^{-1} m^{-1} (Table 3).

The sensitivity analysis of parameters was conducted. The relative errors of the two river sections are shown in Table 4 and Fig. 6. The relative errors of calculation results are less than 10% if the measurement errors are remaining ±1% and ±5% for all parameters. When the measurement errors are ±10% and ±20%, the relative errors of calculation results are less than 27%. When the measurement error is ±35% and +50%, the relative error is mostly less than 50%. The maximum relative error is caused by −50% of the measurement error. In this case, the upstream flow rate C_u and river length L can cause 120.7% and 97.2% of relative error. Therefore, C_u and L can be concluded as sensitive parameters, which coincide with previous studies (Su et al., 2015; Yang et al., 2020).

5. Discussion

5.1. Transformation of rainfall to GW and SW

Stable isotopes (δ^{18}O and δ^2H) are natural indicators for understanding the hydrological mechanisms and pathways by which water travels through the complex system (Binet et al., 2017). Especially for transformations in different water forms, stable isotope values of meteoric waters can be used to trace hydrological processes at different spatial scales (Zhao et al., 2020). The local meteoric water line (LMWL, $\delta^2H = 8.8\ \delta^{18}O + 17.6$, $r^2 = 0.97$, Fig. 3) can be obtained from 126 rainfall samples during 2012 from the Guilin Station reported by Wu et al., (2014). Because Guilin city and the study area are in about 35 km distance and both belong to the Guilin-Yangshuo Basin, with the similar monsoon climate conditions. The LMWL is slightly offset higher than the global meteoric water line (GMWL: $\delta^2H = 8 \times \delta^{18}O + 10$; Craig, 1961). Compared with the GMWL, the steeper slope and higher y-intercept of the LMWL mat be resulted from the relative warm and rainy subtropic climate of the area and less secondary evaporation (Wu et al., 2014). Without the effect of rainfall amount, the δ^{18}O and δ^2H values of rainfall are seasonally changed (depleted to −102‰ for δ^2H and −13.0‰ for δ^{18}O in summer, enriched to 43‰ for δ^2H and 2.5‰ for δ^{18}O in winter) due to the different predominant moisture masses sources (Wu et al., 2014).

Similar to what observed in a mountain catchment of Oregon, USA, the variation of δ^{18}O was primarily related to elevation, which is affected by the prior precipitation (Segura et al., 2019). The depleted δ^{18}O and δ^2H compositions in the Sidi River are likely attributed by the local altitude effect of rainfall in the upstream area, as it was originated from the eastern high mountainous region with almost 800 m elevation difference (Clark and Fritz, 1997). As shown in the blue area of Fig. 3, the δ^{18}O and δ^2H isotopic values in the Sidi River have less variability in different seasons. The enriched stable isotopic compositions of karst groundwater plotted close to the LMWL indicating that the groundwater

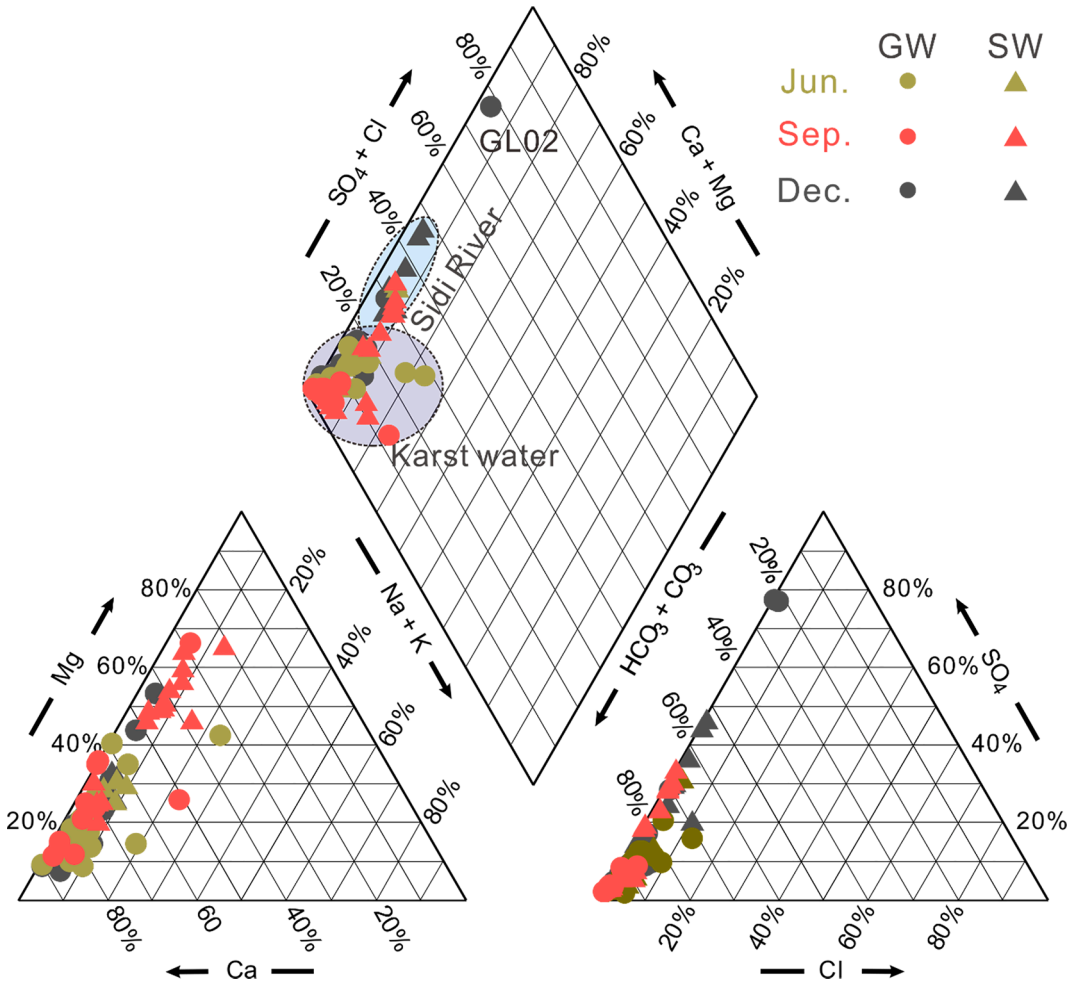

Fig. 2. Piper plot of surface and groundwater samples at different seasons. Solid circles in dark grey, red and green color represent groundwater samples collected during winter, autumn and summer; different color of solid triangles represent surface water samples collected during the correspondent seasons. The light blue ellipse covers most of water collected from the upstream of the Sidi River; the light purple ellipse covers most of samples taken from the downstream karst waters.

may be originated from local rainfall of the downstream karst area (Fig. 3). However, due to the rainfall decreased from summer to winter, the water from the mountainous area (carried with depleted signal) transports through the Sidi River and becomes more and more prevailing as part of recharge to the karst groundwater. It can be indicated by that the $\delta^{18}O$ and $\delta^{2}H$ compositions of karst groundwater get closer to that in winter (Fig. 3) and enriched in summer, depleted in winter. It is opposite to the seasonal pattern of $\delta^{18}O$ and $\delta^{2}H$ in rainfall (Wu et al., 2014; Guo et al., 2015). Moreover, due to the relatively lower hydraulic conductivity, the possibility that the infiltrated rainwater mixed and diffusional exchanged with water stored in the epi-karst from the last season could not be excluded. It results in the different characteristics of $\delta^{18}O$ and $\delta^{2}H$ isotopic compositions in rainfall and groundwater. A similar phenomenon was also observed by previous studies conducted in the Yaji experimental site, a similar karst depression 38 km from the north of the study area (Guo et al., 2015; Chen et al., 2017a, 2017b).

5.2. Surface water-Groundwater exchange

The discharge of the river is sensitive to the net groundwater influent (inflow minus outflow), whereas environmental tracers are sensitive to the gross influent (and effluent) (McCallum et al., 2012). The radon mass balance shows that the influent from groundwater to river occurs in conjunction with river water effluent in both sections. Net gaining and losing sections can be defined based on the variations of river discharge and the radon mass balance.

5.2.1. Net gaining section: R05-R04

The dramatical increase of flow discharge and the drop of ^{222}Rn activities (from 12,150 at R05 to 159.5 Bq/m^3 at R04, with an inflow endmember of 2303.4 Bq/m^3) can be identified as a signal of groundwater influent (Fig. 5 and Table 3). However, stable isotopic values kept in a same level in this section (Fig. 4). The possibility of converging from tributaries was ruled out due to such a growth of flow discharge. Because the inflow of tributaries (e.g. sample R08) can result in isotopic enrichment as they are featured by an elevated signal due to the low elevation. No obvious response for EC values and other major water chemical constituents such as HCO_3^{2-}, SO_4^{2-}, Ca^{2+}, and Mg^{2+} was observed (Figs. 4 and 7). The temperature was also decreased with groundwater inflow, while the DO values slightly increased probably due to the equilibrium with oxygen in the air (Fig. 7).

After a wet season with abundant rainfall, the portion of water stored in the riverbank is characterized by the depleted stable isotopic and EC values of water from the Sidi River. Whereas ^{222}Rn activities are increased in the water of riverbank storage due to the relatively higher solubility in water with a Henry coefficient (ratio of the ^{222}Rn activity (Bq/L) in water versus gas phase) of about 0.35 at 10 °C (Clever, 1979). It is sufficiently supplied by surrounding rocks and soils (Ortega et al., 2017). The pre-stored water was squeezed out to the river driven by the hydraulic gradient from aquifer towards the Sidi River in the section R05-R04. Consequently, only ^{222}Rn activities reacted to the inflow in this section.

Although a partial (or full) contribution of pre-stored water to the

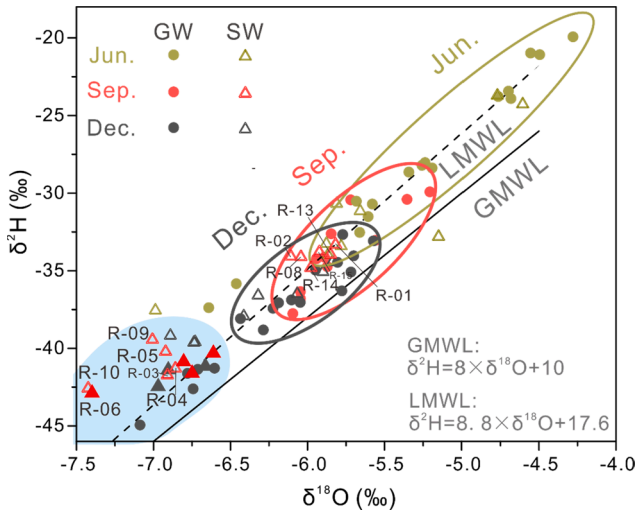

Fig. 3. Plot for showing $\delta^{18}O$ versus $\delta^{2}H$ for surface and karst groundwater in the study area. Solid circles in dark grey, red and green color represent groundwater samples collected during winter, autumn and summer; different color of hollow triangles represent surface water samples collected during the correspondent seasons. Bule are at the bottom-left corner covers most of water collected from the upstream of the Sidi River in all three seasons and groundwater collected from the upstream during winter. There were no groundwater samples taken from the upstream during the other two seasons.

increase of flow discharge in section R05-R04 was inferred, the endmember of inflow water can be assumed to be average value of the samples G02 and S03, as there is a lack of the values from the bank storage water. Inevitably, this part of water contributes to the increase in river discharge could be misinterpreted as groundwater discharge. Therefore, the exchange flux of the section R05-R04 is probably overestimated. Nevertheless, the endmember value obtained from GW samples G02 and S03 can be acceptable due to the following reasons:

1. The well depth of sample G02 is around 1.8 m, which is close to the shallow unsaturated zone, suggesting similar ^{222}Rn activities levels (Batiot-Guilhe et al., 2007). ^{222}Rn activities in S03 is also close to that of the G02.
2. It is well known that ^{222}Rn in the soils is higher than that in limestone (Tadolini and Spizzico, 1998; Laubenstein and Magaldi, 2008). Water in the riverbank contains more ^{222}Rn than that in GW. However, Khadka et al., (2017) revealed a similar and relatively lower ^{222}Rn activities in pore water and small karst springs. It may be

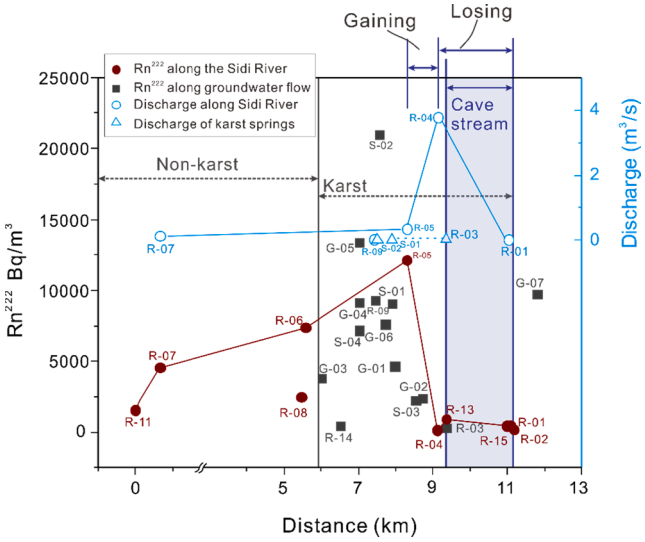

Fig. 5. ^{222}Rn concentration and flow discharge along the Sidi River and groundwater flow direction. Distances are measured downstream of the Pb-Zn mine's tailings pond.

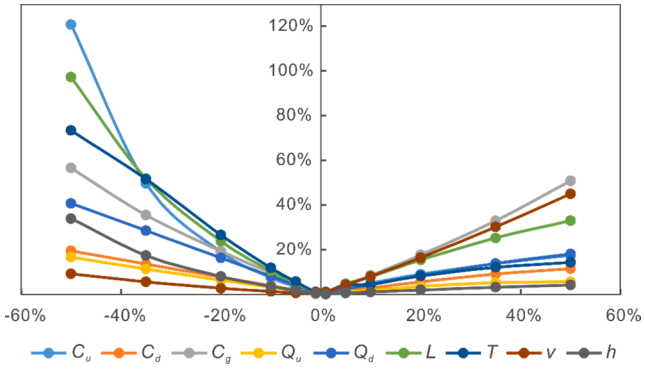

Fig. 6. The relative error of calculated results caused by the measurement error of the parameters. The measurement errors were artificially assigned as ±1% to ±50%

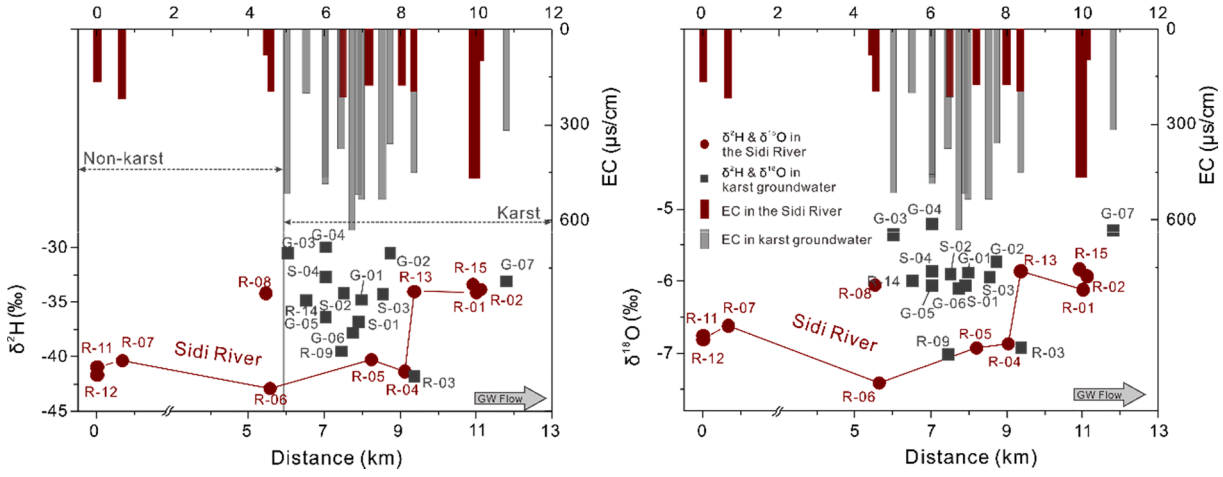

Fig. 4. $\delta^{18}O$ and $\delta^{2}H$ variations along the Sidi River and groundwater flow. Distances are measured downstream of the Pb-Zn mine's tailings pond.

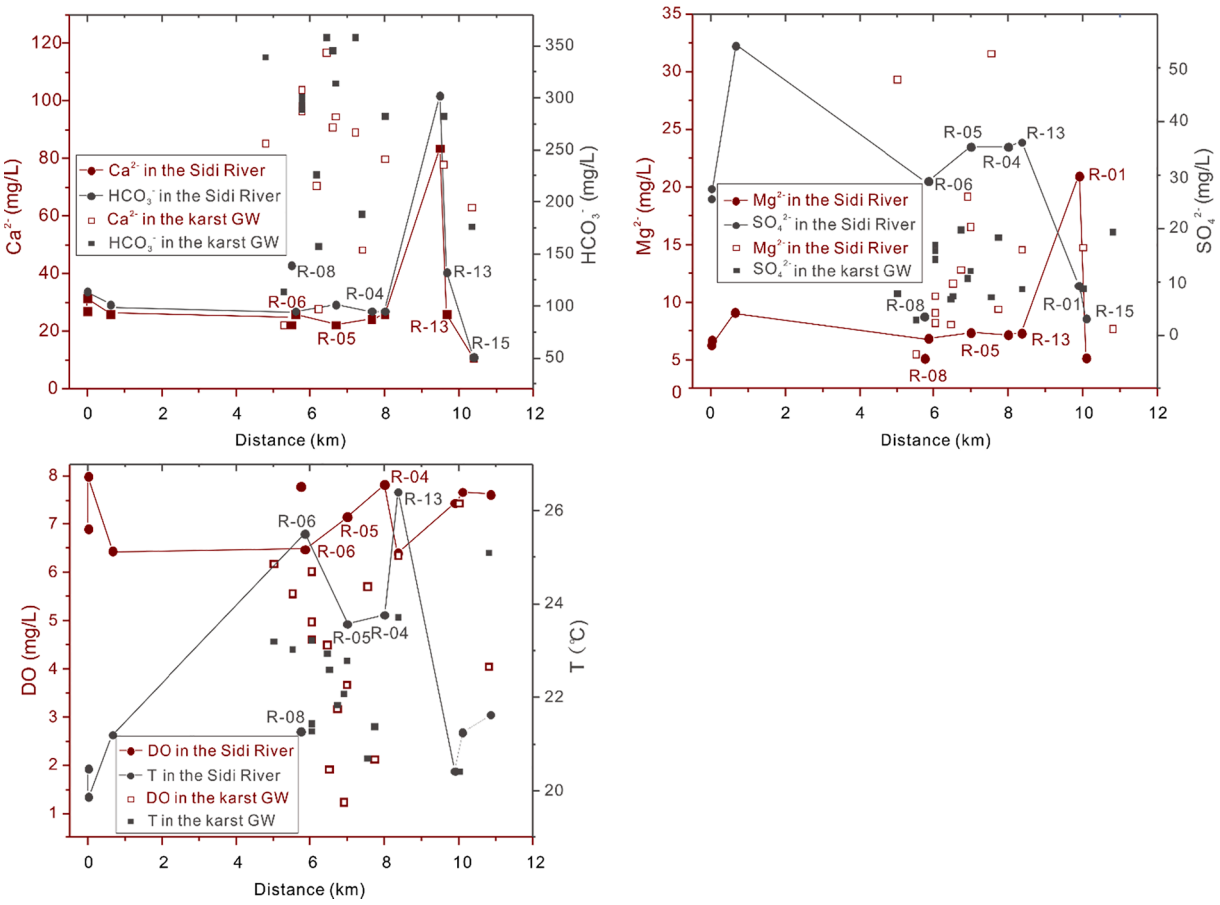

Fig. 7. Physical-chemical indicators in waters along the Sidi River and groundwater flow.

resulted from that the diffuse flow through the porous medium is slow enough allowing ^{222}Rn to decay.

Hence, it can be assumed the similar ^{222}Rn activities of the bank storage water with that in the shallow GW. The resulting exchange flux q_g represents the water contributed both by the bank storage and the karst aquifer. The relative error of inflow endmember will be discussed in the following section.

It is basically equivalent for the fluxes in both directions (q_g and q_r) as they are in the same order of magnitude in the section R05-R04. Generally, such recharge from the riverbank storage is taking place when there are rise and subsequent fall in the river stage (Cranswick and Cook, 2015). Frequently, surface water loses to its bank, reducing the flood level and recharging the aquifer during flood event. When a dry season comes, the pre-stored bank storage water releases to compensate the decrease of river flow (Sophocleous, 2002). Sometimes under the baseflow conditions, the amount of bank storage water can even surpass the discharge of groundwater (Brunke and Gonser, 1997). Karst area usually are considered as relatively poor systems of regulation but strong systems of amplification or generation of floods and flash floods (Bailly-Comte et al., 2012), in which epi-karst exerts a strong control on run-off generation (Fu et al., 2016). Poulain et al., (2018) observed that the diffuse flow dominates most of the storage water in the low permeability epi-karst zones. In this study, the variations of EC, δ^{18}O and δ^{2}H, and ^{222}Rn activities corresponding to the increase of river flow can be resulted from the of antecedent stored water discharge (Deng et al., 2017).

5.2.2. Net losing section: R04-R01

Over 99% of river flow is lost in section R04-R01 when it flows through the section R04-R01. Therefore, q_r is relative dominant as it is one order of magnitude larger than q_g in the section R04-R01 (Table 3). The segment of conduit (R13-R01) potentially plays a critical role in the loss of a large amount of water as it accounts for almost half of the section and with a higher hydraulic conductivity (Fig. 1).

Tracers vary in the segment from R04 to R13 and in the segment of the conduit (from R13 to R01). The enriched δ^{18}O and δ^{2}H values in the Sidi River relative to the stable isotopic levels of GW indicate the inflow of GW in R04 to R13 and remain the values in R13 to R01. As mentioned above in section 3.2.2, the total evaporation loss accounts for about 2% of the river depth within around 5 days. Besides, in Fig. 3, both surface- and ground-water are close to the LMWL or slightly higher than it, usually presenting a signal of evaporation. The distance from R04 to R13 is around 500 m, with an average flow rate of 0.72 m/s (Table 3). The river water allows to stay less than half an hour. As a result of the stable isotopic values enrichment from R04 to R13, the effect of evaporation could be neglected.

Except for the stable isotopic values, no obvious variation has been observed for chemicals (EC, HCO_3^{2-}, SO_4^{2-}, Ca^{2+}, and Mg^{2+}), T and DO in the segment from R04 to R13. It might be resulted from the short residence time, thus the chemical-physical indexes could not be evenly distributed. In contrast, the mixing of different waters can be seen from a dramatically declined temperature and being close to the similar hydrochemical levels with those in karst groundwater (Fig. 7). The inconsistent responses of different tracers at different parts of the section R04-R01 reflect the intensity and complexity of the conduit in SW-GW interaction of karst areas.

5.3. Conceptual model of Rainfall-SW-GW transformation processes

The quality of surface- and ground-water of the study area has been threatened by the upstream Pb-Zn mine and its tailings (Kong et al.,

2018; Qin et al., 2019). It is essential to obtain the knowledge of water transformations from rainfall to surface- and ground-water, as well as accurately quantify the interaction between surface- and ground-water. Based on above observations a conceptual model of the rainfall-SW-GW transformation regime is constructed in the subtropical karst area of Southwest China. This model presents several major processes responsible for transformations in different water forms in the study area. These are as follows: (1) An obvious altitude effect on the $\delta^{18}O$ and $\delta^{2}H$ isotopic values in the upstream non-karst area has been observed; (2) For the recharge of karst groundwater in the downstream valley, water originated from the upstream non-karst area with the depleted stable isotopic signal and transported through the Sidi River is dominant in winter; The local rainfall water characterized by the elevated stable isotopic signal is more important during summertime; (3) In the gaining section of the karst area, the bank storage water superimposed on karst groundwater contributes to the increase of flow discharge, and the quantities of inflow and outflow are in the same order of magnitude; (4) In the following losing section, a well-mixing process between river water and groundwater has been observed in the segment of conduit, which indicates the different variations of tracers relative to the segment of surface flow. The amount of outflow is one order of magnitude larger than that of inflow.

5.4. Environmental implications

Abandoned metal(s) mines and their related tailings are widely distributed in southwest China (Kun et al., 2016; Chen et al., 2017a, 2017b; Lu et al., 2019), which is one of the most developed karst landscapes in the world. The study area has long suffered from heavy metals in soil. However, there is less attention has been paid to the quality of surface water and groundwater (Qin et al., 2019). Previous research on the effect of the abandoned Pb-Zn mine on the karst water showing there is potentially transport of heavy metals such as Pb, Zn, Cd and As through the Sidi River (Qin et al., 2019). Among all the three seasons, SO_4^{2-} is the most dominant in winter (Dec. 2015) as it accounts for more than 40% of total anions in three of surface water samples, and it accounts for 78% of the total anions in the mine drainage water (Fig. 2, Qin et al., 2019). The SO_4^{2-} ion varies in an inverse characteristic (higher in the Sidi river and lower in GW, Fig. 6) compared with other hydrochemicals. It may be resulted from sulfides oxidation from the mine and tailings. The sulfides oxygenation can release large quantities of metals to the downstream karst valley transported by the Sidi River (Qin et al., 2019). During the bank storage water intrusion, the transported organic matter can induce carbonate dissolution, alters redox state, and impacts trace metal mobility (Brown et al., 2014, 2019). Metals thus are introduced into GW through SW-GW interaction, especially through conduit flow, in which water could exchange back and forth directly. A study in a similar mountain area of south China, the Dabaoshan Mine Area, manifested that hydraulic transportation can be the most important driving force for metallic elements migration in both dissolved phase and fine suspended particle phase (Chen et al., 2018). Actually, river water recharge could transport heavy metals into the surrounding aquifers as well in both dry and wet seasons (Wang et al., 2019). In the Dabaoshan mine area, the contaminated aquifer due to the discharge of acid mine drainage is, in turn, acting as long-term significant pollution sources to the surrounding gaining rivers (Wang et al., 2019). Therefore, it is urgent to put more efforts on the study of water quality and transport of metals in the presented karst water system.

6. Conclusions

Transformations of rainfall-surface water-groundwater are important for water resources regulation and further tracing the transport of potential contaminations (such as Pb, Zn, Cd and Gu) in the historical polluted karst system. The transformation processes have been identified based on the $\delta^{2}H$ and $\delta^{18}O$ isotopic compositions, physical and chemical indexes (T, DO, EC, HCO_3^{2-}, SO_4^{2-}, Ca^{2+}, and Mg^{2+}) and ^{222}Rn activities in different water forms. $\delta^{18}O$ and $\delta^{2}H$ in rainfall on the upstream non-karst area and downstream karst area are characterized with different values due to the altitude effect, which makes the Sidi River from the upstream carrying a depleted signal. The $\delta^{18}O$ and $\delta^{2}H$ levels in karst GW vary during summer-autumn–winter seasons, showing the dominant recharge from the river to the karst groundwater in winter and less dominant during summer.

Interaction between the Sidi River and GW in the downstream karst area was estimated according to the ^{222}Rn mass balance model superimposed on the information obtained from river flow gauging, $\delta^{18}O$ and $\delta^{2}H$ stable isotope values, and the physical–chemical items in autumn. A net gaining section ($q_n = 3.58 \times 10^{-3}$ $m^3/s/m$) and a net losing section ($q_n = 3.95 \times 10^{-3}$ $m^3/s/m$) have been delineated and quantified. The bank storage water contributed in the net gaining section, reflected by the inconsistent of spatial responses of stable isotopic and chemical tracers to the GW influent, which resulted in a relative identical amount of groundwater inflow and river water outflow (q_g and q_r are 3.58×10^{-3} and 1.43×10^{-3} $m^3/s/m$ respectively). The outflow of river water ($q_r = 4.23 \times 10^{-3}$ $m^3/s/m$) is one order of magnitude larger than the inflow of groundwater ($q_g = 2.80 \times 10^{-4}$) in the net losing section, in which a well-mixing process can be observed in the conduit segment.

Toxic metals both in dissolved phase and suspended particle phase may be introduced to the water system along with the processes of rainfall to SW and GW, and easily transported throughout the system as the intense SW-GW interaction. Both this and the previous study have revealed the unusual variation characteristic of SO_4^{2-} ion, which probably is a result of sulfides oxygenation from the mine and tailings. We recommend continued monitoring of SW and GW quality, and further evaluating the transport of metals in the rainfall-SW-GW processes, as well as duly reinforce of the tailings dam and remediation of contaminated soil to prevent the continual release of toxic metals.

CRediT authorship contribution statement

Wenjing Qin: Conceptualization, Methodology, Formal analysis, Writing - original draft, Writing - review & editing, Methodology, Validation, Investigation. **Dongmei Han:** Conceptualization, Writing - review & editing, Funding acquisition, Project administration. **Xianfang Song:** Conceptualization, Supervision, Resources. **Shaohua Liu:** Investigation, Visualization, Resources.

Declaration of Competing Interest

The authors declare that they have no known competing financial interests or personal relationships that could have appeared to influence the work reported in this paper.

Acknowledgement

This study was supported by the Outstanding Member Program of the Youth Innovation Promotion Association, Chinese Academy of Sciences (grant number 2012040), and the Project of China Geological Survey (DD20190502) titled ‘Comprehensive geological survey and evaluation of rocky desertification in key areas of south China’.

References

Aghili, S., Vaezihir, A., Hosseinzadeh, M., 2018. Distribution and modeling of heavy metal pollution in the sediment and water mediums of Pakhir River, at the downstream of Sungun mine tailing dump, Iran. Environ. Earth Sci. 77 (4) https://doi.org/10.1007/s12665-018-7283-z.

Arnoux, M., Gibert-Brunet, E., Barbecot, F., Guillon, S., Gibson, J., Noret, A., 2017. Interactions between groundwater and seasonally ice-covered lakes: using water stable isotopes and radon-222 multilayer mass balance models. Hydrol. Process. 31 (14), 2566–2581. https://doi.org/10.1002/hyp.11206.

Atkinson, A.P., Cartwright, I., Gilfedder, B.S., Hofmann, H., Unland, N.P., Cendón, D.I., Chisari, R., 2015. A multi-tracer approach to quantifying groundwater inflows to an

upland river; assessing the influence of variable groundwater chemistry: a multi-tracer approach to quantifying groundwater. Hydrol. Process. 29 (1), 1–12. https://doi.org/10.1002/hyp.10122.
Bailly-Comte, V., Borrell-Estupina, V., Jourde, H., Pistre, S., 2012. A conceptual semidistributed model of the Coulazou River as a tool for assessing surface water-karst groundwater interactions during flood in Mediterranean ephemeral rivers: karst contribution to surface floW. Water Resour. Res. 48 (9) https://doi.org/10.1029/2010WR010072.
Bailly-Comte, V., Jourde, H., Pistre, S., 2009. Conceptualization and classification of groundwater–surface water hydrodynamic interactions in karst watersheds: case of the karst watershed of the Coulazou River (Southern France). J. Hydrol. 376 (3-4), 456–462. https://doi.org/10.1016/j.jhydrol.2009.07.053.
Batiot-Guilhe, C., Seidel, J.-L., Jourde, H., Hébrard, O., Bailly-Comte, V., 2007. Seasonal variations of CO_2 and ^{222}Rn in a mediterranean sinkhole - spring (Causse d'Aumelas, SE France). Int. J. Speleol. 36 https://doi.org/10.5038/1827-806X.36.1.5.
Bhat, N.A., Jeelani, G.h., 2018. Quantification of groundwater–surface water interactions using environmental isotopes: a case study of Bringi Watershed, Kashmir Himalayas, India. J. Earth Syst. Sci. 127 (5) https://doi.org/10.1007/s12040-018-0964-x.
Binet, S., Joigneaux, E., Pauwels, H., Albéric, P., Fléhoc, C.h., Bruand, A., 2017. Water exchange, mixing and transient storage between a saturated karstic conduit and the surrounding aquifer: Groundwater flow modeling and inputs from stable water isotopes. J. Hydrol. 544, 278–289. https://doi.org/10.1016/j.jhydrol.2016.11.042.
Broecker Tracers in the Sea, 1982. Eldigio Press, Palisades, N.Y.
Brown, A.L., Martin, J.B., Kamenov, G.D., Ezell, J.E., Screaton, E.J., Gulley, J., Spellman, P., 2019. Trace metal cycling in karst aquifers subject to periodic river water intrusion. Chem. Geol. 527, 118773. https://doi.org/10.1016/j.chemgeo.2018.05.020.
Brown, A.L., Martin, J.B., Screaton, E.J., Ezell, J.E., Spellman, P., Gulley, J., 2014. Bank storage in karst aquifers: the impact of temporary intrusion of river water on carbonate dissolution and trace metal mobility. Chem. Geol. 385, 56–69. https://doi.org/10.1016/j.chemgeo.2014.06.015.
Brunke, M., Gonser, T., 1997. The ecological significance of exchange processes between rivers and groundwater. Freshw. Biol. 37 (1), 1–33. https://doi.org/10.1046/j.1365-2427.1997.00143.x.
Charlier, J.-B., Moussa, R., Pinson, S., Narbaïs, D., Desprats, J.-F., 2019. Recent advances on the characterization of karst-river interactions during floods. In: Presented at the 27th International Karstological School - "Classical Karst.".
Chen, H., Hu, K.e., Nie, Y., Wang, K., 2017a. Analysis of soil water movement inside a footslope and a depression in a karst catchment, Southwest China. Sci. Rep. 7 (1) https://doi.org/10.1038/s41598-017-02619-x.
Chen, M., Lu, G., Wu, J., Yang, C., Niu, X., Tao, X., Shi, Z., Yi, X., Dang, Z., 2018. Migration and fate of metallic elements in a waste mud impoundment and affected river downstream: A case study in Dabaoshan Mine, South China. Ecotoxicol. Environ. Saf. 164, 474–483. https://doi.org/10.1016/j.ecoenv.2018.08.063.
Chen, Z., Auler, A.S., Bakalowicz, M., Drew, D., Griger, F., Hartmann, J., Jiang, G., Moosdorf, N., Richts, A., Stevanovic, Z., Veni, G., Goldscheider, N., 2017b. The World Karst Aquifer Mapping project: concept, mapping procedure and map of Europe. Hydrogeol. J. 25 (3), 771–785. https://doi.org/10.1007/s10040-016-1519-3.
Chu, H., Wei, J., Wang, R., Xin, B., 2017. Characterizing the interaction of groundwater and surface water in the karst aquifer of Fangshan, Beijing (China). Hydrogeol. J. 25 (2), 575–588. https://doi.org/10.1007/s10040-016-1507-7.
Clark, I.D., Fritz, P., 1997. Environmental Isotopes in Hydrogeology. CRC Press.
Clever, H.L., 1979. Krypton, Xenon & Radon- Gas Solubilities IUPAC Solubility Data Series 2. Pergamon Press, Oxford.
Close, M., Matthews, M., Burbery, L., Abraham, P., Scott, D., 2014. Use of radon to characterise surface water recharge to groundwater. J. Hydrol. N. Z. 53, 113–127.
Cook, P.G., 2013. Estimating groundwater discharge to rivers from river chemistry surveys: groundwater discharge to rivers. Hydrol. Process. 27 (25), 3694–3707. https://doi.org/10.1002/hyp.9493.
Cook, P.G., Favreau, G., Dighton, J.C., Tickell, S., 2003. Determining natural groundwater influx to a tropical river using radon, chlorofluorocarbons and ionic environmental tracers. J. Hydrol. 277 (1-2), 74–88. https://doi.org/10.1016/S0022-1694(03)00087-8.
Cook, P.G., Lamontagne, S., Berhane, D., Clark, J.F., 2006. Quantifying groundwater discharge to Cockburn River, southeastern Australia, using dissolved gas tracers 222 Rn and SF 6. Water Resour. Res. 42 (10) https://doi.org/10.1029/2006WR004921.
Craig, H., 1961. Isotopic variations in meteoric waters. Science 133 (3465), 1702–1703. https://doi.org/10.1126/science:133.3465.1702.
Cranswick, R.H., Cook, P.G., 2015. Scales and magnitude of hyporheic, river-aquifer and bank storage exchange fluxes. Hydrol. Process. 29 (14), 3084–3097. https://doi.org/10.1002/hyp.10421.
Danckwerts, P.V., 1951. Significance of liquid-film coefficients in gas absorption. Ind. Eng. Chem. 43 (6), 1460–1467. https://doi.org/10.1021/ie50498a055.
Deng, Y., Jiang, Z., Hu, Y., Zhou, X., Li, Y., Tao, H., 2017. Response of Ecological pattern/process to epikarst water on typical karst critical zone in Southwest (Research No. 400002574– YYWF201401/6). Institute of Karst Geology, Chinese Academy of Geological Sciences.
Ellins, K.K., Roman-Mas, A., Lee, R., 1990. Using 222Rn to examine groundwater/surface discharge interaction in the Rio Grande de Manati, Puerto Rico. J. Hydrol. 115 (1-4), 319–341. https://doi.org/10.1016/0022-1694(90)90212-G.
Folger, P.F., Poeter, E., Wantye, R.B., Day, W., Frishman, D., 1997. 222Rn transport in a fractured crystalline rock aquifer: results from numerical simulations. J. Hydrol. 195 (1-4), 45–77. https://doi.org/10.1016/S0022-1694(96)03243-X.
Ford, D., Williams, P.D., 2007. Karst Hydrogeology and Geomorphology. John Wiley & Sons.
Fu, Z., Chen, H., Xu, Q., Jia, J., Wang, S., Wang, K., 2016. Role of epikarst in near-surface hydrological processes in a soil mantled subtropical dolomite karst slope: implications of field rainfall simulation experiments. Hydrol. Process. 30 (5), 795–811. https://doi.org/10.1002/hyp.10650.
Guo, X., Jiang, G., Gong, X., Yin, J., Wu, X., 2015. Recharge processes on typical karst slopes implied by isotopic and hydrochemical indexes in Xiaoyan Cave, Guilin, China. J. Hydrol. 530, 612–622. https://doi.org/10.1016/j.jhydrol.2015.09.065.
Gutiérrez, M., Mickus, K., Camacho, L.M., 2016. Abandoned Pb Zn mining wastes and their mobility as proxy to toxicity: a review. Sci. Total Environ. 565, 392–400. https://doi.org/10.1016/j.scitotenv.2016.04.143.
Herschy, R.W., 1998. In: Encyclopedia of Earth ScienceHydrology and Lakes. Kluwer Academic Publishers, Dordrecht, pp. 668–670. https://doi.org/10.1007/1-4020-4513-1_228.
Institute of Karst Geology, 2015. Hydrogeological Survey Report For Guangxi Zhuang Autonomous Region. China Geological Survey.
Jie, W., 2007. Application of environmental isotopes to the study on precipitation-surface water-groundwater transformation. Geotech. Investig. Surv. 3.
Jin, Z., Li, Z., Li, Q., Hu, Q., Yang, R., Tang, H., Li, M., Huang, B., Zhang, J., Li, G., 2015. Canonical correspondence analysis of soil heavy metal pollution, microflora and enzyme activities in the Pb–Zn mine tailing dam collapse area of Sidi village, SW China. Environ. Earth Sci. 73 (1), 267–274. https://doi.org/10.1007/s12665-014-3421-4.
Khadka, M.B., Martin, J.B., Kurz, M.J., 2017. Synoptic estimates of diffuse groundwater seepage to a spring-fed karst river at high spatial resolution using an automated radon measurement technique. J. Hydrol. 544, 86–96. https://doi.org/10.1016/j.jhydrol.2016.11.013.
Kong, J., Guo, Q., Wei, R., Strauss, H., Zhu, G., Li, S., Song, Z., Chen, T., Song, B.o., Zhou, T., Zheng, G., 2018. Contamination of heavy metals and isotopic tracing of Pb in surface and profile soils in a polluted farmland from a typical karst area in southern China. Sci. Total Environ. 637-638, 1035–1045. https://doi.org/10.1016/j.scitotenv.2018.05.034.
Kun, R., Zhibing, C., Xiaodong, P., Mei, Z., 2016. Environmental geochemistry characteristics of heavy metals and ecological risk assessment of surface sediments from Nanshan Laolongdong subterranean river, Chongqing. Carsologica Sin. 35, 144–152.
Laubenstein, M., Magaldi, D., 2008. Natural radioactivity of some red Mediterranean soils. CATENA 76 (1), 22–26. https://doi.org/10.1016/j.catena.2008.08.005.
Lenhart, T., Eckhardt, K., Fohrer, N., Frede, H.-G., 2002. Comparison of two different approaches of sensitivity analysis. Phys. Chem. Earth, Parts A/B/C 27 (9-10), 645–654. https://doi.org/10.1016/S1474-7065(02)00049-9.
Lewis, W.K., Whitman, W.G., 1924. Principles of gas absorption. Ind. Eng. Chem. 16 (12), 1215–1220. https://doi.org/10.1021/ie50180a002.
Li, Q., Hu, Q., Zhang, C., Müller, W.E.G., Schröder, H.C., Li, Z., Zhang, Y., Liu, C., Jin, Z., 2015. The effect of toxicity of heavy metals contained in tailing sands on the organic carbon metabolic activity of soil microorganisms from different land use types in the karst region. Environ. Earth Sci. 74 (9), 6747–6756. https://doi.org/10.1007/s12665-015-4684-0.
Li, Z., Ma, Z., van der Kuijp, T.J., Yuan, Z., Huang, L., 2014. A review of soil heavy metal pollution from mines in China: pollution and health risk assessment. Sci. Total Environ. 468-469, 843–853. https://doi.org/10.1016/j.scitotenv.2013.08.090.
Lin, B., 1997. Study on cadmium pollution of soil - crop in a lead - zinc mine area. Chin. J. Soil Sci. 28, 235–237.
Lin, B., 1995. Initiatory study of the pollutiong of cadmium in soil in Pb-Zn mining area. J. Guilin Inst. Technol. 15, 66–69.
Lu, Q., Wang, S., Bai, X., Liu, F., Wang, M., Wang, J., Tian, S., 2019. Rapid inversion of heavy metal concentration in karst grain producing areas based on hyperspectral bands associated with soil components. Microchem. J. 148, 404–411. https://doi.org/10.1016/j.microc.2019.05.031.
McCallum, J.L., Cook, P.G., Berhane, D., Rumpf, C., McMahon, G.A., 2012. Quantifying groundwater flows to streams using differential flow gaugings and water chemistry. J. Hydrol. 416-417, 118–132. https://doi.org/10.1016/j.jhydrol.2011.11.040.
Mikkelsen, P.S., Häfliger, M., Ochs, M., Jacobsen, P., Tjell, J.C., Boller, M., 1997. Pollution of soil and groundwater from infiltration of highly contaminated stormwater – a case study. Water Sci. Technol. 36, 325–330. https://doi.org/10.1016/S0273-1223(97)00578-7.
National Standard of the People's Republic of China, 2015. GB15618-1995: Environmental quality standard for soils. <https://www.chinesestandard.net>.
O'Connor, D.J., Dobbins, W.E., 1958. Mechanism of reaeration in natural streams. Trans. Am. Soc. Civ. Eng. 123, 641–666.
Ortega, L., Manzano, M., Custodio, E., Hornero, J., Rodríguez-Arévalo, J., 2015. Using 222Rn to identify and quantify groundwater inflows to the Mundo River (SE Spain). Chem. Geol. 395, 67–79. https://doi.org/10.1016/j.chemgeo.2014.12.002.
Ortega, L., Manzano, M., Rodríguez-Arévalo, J., 2017. Testing the usefulness of 222Rn to complement conventional hydrochemical data to trace groundwater provenance in complex multi-layered aquifers. Application to the Úbeda aquifer system (Jaén, SE Spain). Sci. Total Environ. 599, 2105–2120. https://doi.org/10.1016/j.scitotenv.2017.04.056.
Padilla, I.Y., Vesper, D.J., 2018. Fate, Transport, and exposure of emerging and legacy contaminants in karst systems: state of knowledge and uncertainty. In: Karst Groundwater Contamination and Public Health, Advances in Karst Science. Springer, Cham, pp. 33–49. https://doi.org/10.1007/978-3-319-51070-5_5.
Parise, M., Gabrovsek, F., Kaufmann, G., Ravbar, N., 2018. Recent advances in karst research: from theory to fieldwork and applications. Geol. Soc., London, Spec. Publ. 466 (1), 1–24. https://doi.org/10.1144/SP466.26.
Poulain, A., Watlet, A., Kaufmann, O., Van Camp, M., Jourde, H., Mazzilli, N., Rochez, G., Deleu, R., Quinif, Y., Hallet, V., 2018. Assessment of groundwater

recharge processes through karst vadose zone by cave percolation monitoring. Hydrol. Process. 32 (13), 2069–2083. https://doi.org/10.1002/hyp.13138.
Qin, W., Han, D., Song, X., Engesgaard, P., 2019. Effects of an abandoned Pb-Zn mine on a karstic groundwater reservoir. J. Geochem. Explor. 200, 221–233. https://doi.org/10.1016/j.gexplo.2018.09.007.
Rößler, F.A., Villert, J., 2017. On-site determination of the radon concentration in water: sampling & on-line methods.
Rugel, K., Golladay, S.W., Jackson, C.R., Rasmussen, T.C., 2016. Delineating groundwater/surface water interaction in a karst watershed: Lower Flint River Basin, southwestern Georgia, USA. J. Hydrol.: Reg. Stud. 5, 1–19. https://doi.org/10.1016/j.ejrh.2015.11.011.
Segura, C., Noone, D., Warren, D., Jones, J.A., Tenny, J., Ganio, L.M., 2019. Climate, landforms, and geology affect baseflow sources in a mountain catchment. Water Resour. Res. 55 (7), 5238–5254. https://doi.org/10.1029/2018WR023551.
Sophocleous, M., 2002. Interactions between groundwater and surface water: the state of the science. Hydrogeol. J. 10 (1), 52–67. https://doi.org/10.1007/s10040-001-0170-8.
Stellato, L., Petrella, E., Terrasi, F., Belloni, P., Belli, M., Sansone, U., Celico, F., 2008. Some limitations in using 222Rn to assess river–groundwater interactions: the case of Castel di Sangro alluvial plain (central Italy). Hydrogeol. J. 16 (4), 701–712. https://doi.org/10.1007/s10040-007-0263-0.
Su, X., Xu, W., Yang, F., Zhu, P., 2015. Using new mass balance methods to estimate gross surface water and groundwater exchange with naturally occurring tracer 222 Rn in data poor regions: a case study in northwest China. Hydrol. Process. 29 (6), 979–990. https://doi.org/10.1002/hyp.10208.
Sun, J., Tang, C., Wu, P., Strosnider, W.H.J., Han, Z., 2013. Hydrogeochemical characteristics of streams with and without acid mine drainage impacts: a paired catchment study in karst geology, SW China. J. Hydrol. 504, 115–124. https://doi.org/10.1016/j.jhydrol.2013.09.029.
Tadolini, T., Spizzico, M., 1998. Relation between "terra rossa" from the Apulia aquifer of Italy and the radon content of groundwater: experimental results and their applicability to radon occurrence in the aquifer. Hydrogeol. J. 6 (3), 450–454. https://doi.org/10.1007/s100400050167.
Tóth, J., 1970. A conceptual model of the groundwater regime and the hydrogeologic environment. J. Hydrol. 10 (2), 164–176. https://doi.org/10.1016/0022-1694(70)90186-1.
UNESCO World Heritage Centre, 2007. South China Karst [WWW Document]. UNESCO World Herit. Cent. URL <https://whc.unesco.org/en/list/1248/> (accessed 2.21.20).
Vesper, D.J., 2019. Chapter 36 - contamination of cave waters by heavy metals. In: White, W.B., Culver, D.C., Pipan, T. (Eds.), Encyclopedia of Caves, third ed. Academic Press, pp. 320–325. https://doi.org/10.1016/B978-0-12-814124-3.00035-2.
Wang, Y.a., Dong, R., Zhou, Y., Luo, X., 2019. Characteristics of groundwater discharge to river and related heavy metal transportation in a mountain mining area of Dabaoshan, Southern China. Sci. Total Environ. 679, 346–358. https://doi.org/10.1016/j.scitotenv.2019.04.273.
Wijngaard, R.R., van der Perk, M., van der Grift, B., de Nijs, T.C.M., Bierkens, M.F.P., 2017. The Impact of climate change on metal transport in a lowland catchment. Water Air Soil Pollut. 228 (3) https://doi.org/10.1007/s11270-017-3261-4.
Wu, X., Zhu, X., Pan, M., Zhang, M., 2014. Seasonal variability of oxygen and hydrogen stable isotopes in precipitation and cave drip water at Guilin, southwest China. Environ. Earth Sci. 72 (8), 3183–3191. https://doi.org/10.1007/s12665-014-3224-7.
Xiao, K., Li, H., Shananan, M., Zhang, X., Wang, X., Zhang, Y., Zhang, X., Liu, H., 2019. Coastal water quality assessment and groundwater transport in a subtropical mangrove swamp in Daya Bay, China. Sci. Total Environ. 646, 1419–1432. https://doi.org/10.1016/j.scitotenv.2018.07.394.
Yang, J., Yu, Z., Yi, P., Frape, S.K., Gong, M., Zhang, Y., 2020. Evaluation of surface water and groundwater interactions in the upstream of Kui river and Yunlong lake, Xuzhou, China. J. Hydrol. 583, 124549. https://doi.org/10.1016/j.jhydrol.2020.124549.
Yuan, D., Drogue, C., Dai, A., Lao, W., Cai, W., Bidaux, P., Razack, M., 1990. Hydrology of the Karst aquifer at the experimental site of Guilin in southern China. J. Hydrol. 115, 285–296. https://doi.org/10.1016/0022-1694(90)90210-O.
Zhao, B., Li, Z., Li, P., Cheng, Y., Gao, B., 2020. Effects of ecological construction on the transformation of different water types on Loess Plateau, China. Ecol. Eng. 144, 105642. https://doi.org/10.1016/j.ecoleng.2019.105642.
Zhao, D., Wang, G., Liao, F.u., Yang, N., Jiang, W., Guo, L., Liu, C., Shi, Z., 2018. Groundwater-surface water interactions derived by hydrochemical and isotopic (222Rn, deuterium, oxygen-18) tracers in the Nomhon area, Qaidam Basin, NW China. J. Hydrol. 565, 650–661. https://doi.org/10.1016/j.jhydrol.2018.08.066.